Calcium diffusion modeling in a spherical neuron

Relevance of buffering properties

Francisco Sala and Arturo Hernández-Cruz
Howard Hughes Medical Institute, Department of Neurobiology and Behavior, State University of New York, Stony Brook, New York 11794

ABSTRACT We have developed a calcium diffusion model for a spherical neuron which incorporates calcium influx and extrusion through the plasma membrane as well as three calcium buffer systems with different capacities, mobilities, and kinetics. The model allows us to calculate the concentration of any of the species involved at all locations in the cell and can be used to account for experimental data obtained with high-speed Ca imaging techniques. The influence of several factors on the Ca^{2+} transients is studied. The relationship between peak $[Ca^{2+}]_i$ and calcium load is shown to be nonlinear and to depend on buffer characteristics. The time course of the Ca^{2+} signals is also shown to be dependent on buffer properties. In particular, buffer mobility strongly determines the size and time course of Ca^{2+} signals in the cell interior. The model predicts that the presence of exogenous buffer, such as fura-2, modifies the Ca^{2+} transients to a variable extent depending on its proportion relative to the natural, intrinsic buffers. The conclusions about natural calcium buffer properties that can be derived from Ca imaging experiments are discussed.

INTRODUCTION

Intracellular Ca^{2+} has been proposed to play a pivotal role in a number of events, including transmitter release (Katz and Miledi, 1967; Llinás et al., 1981), intracellular calcium release (Fabiato, 1983; Lipscombe et al., 1988*b*), control of membrane permeability (Meech, 1978; Aschcroft and Stanfield, 1981) and activation of enzymes and genes (Rasmussen and Barrett, 1984; Morgan and Curran, 1988). A detailed knowledge of intracellular $[Ca^{2+}]$ spread is essential to understand the function of calcium as an intracellular messenger. Conventional techniques for measuring $[Ca^{2+}]_i$ lack both the spatial and temporal resolution required to visualize the highly localized calcium fluxes accompanying subcellular calcium signaling. However, high-speed Ca^{2+} imaging using confocal microscopy and long-wavelength Ca^{2+} indicators provides a powerful tool to begin studying the dynamics of calcium in the micrometer and millisecond ranges (Hernández-Cruz et al., 1989*a*, and *b*).

To account for the calcium movements monitored with confocal microscopy in bullfrog sympathetic neurons, we formulated a diffusion model for a spherical cell incorporating three different buffer systems as well as Ca entry and extrusion through the plasma membrane. In this report we describe how the model can be used to explore the influence of factors that combine to shape calcium signals at different locations in the cell. Among these factors, the characteristics of the intrinsic buffers (i.e., mobility, capacity, and kinetics) and of the rates of calcium extrusion were found to modify the distribution of $[Ca^{2+}]_i$ to different extents. We also examined the effect of introducing Ca^{2+} indicators, which act as Ca buffers themselves. The extent to what the physiological responses can be distorted by the presence of the indicator and the consequences of that distortion for conclusions derived from this type of experiment are discussed.

Dr. Sala's present address is Departamento de Neuroquímica, Universidad de Alicante, Alicante, Spain.

Dr. Hernández-Cruz's present address is Dept. of Neurosciences, Roche Institute of Molecular Biology, 340 Kingsland St., Nutley, NJ 07110-1199.

METHODS

Diffusion

This model takes into account several different species (S), namely Ca^{2+} and either two or three buffer systems (B_1, B_2, and B_3) in both their free and Ca-bound forms. If tangential components of diffusion are neglected, then the three-dimensional diffusion equations in a sphere can be reduced to a one-dimensional equation (Crank, 1975). The general diffusion equation for all species can be written as:

$$\delta(r[S])/\delta t = D_S \cdot (\delta^2 r[S])/\delta r^2), \quad (1)$$

where [S] is the concentration of the species, D_S is its diffusion coefficient, and r is the distance from the center of the sphere.

Discretization in both space and time is required to solve Eq. 1. The model consists of forty concentric shells 0.5 μm in thickness each. Calculation of the concentration of all species at any given time and for every shell is then possible.

A finite difference approximation (first order Euler scheme) was used

0006-3495/90/02/313/12 $2.00

to solve numerically the partial differential equations with Δx and Δt small enough to assure stability and convergence (Smith, 1985). Thus, for each shell centered on r and for all diffusable species, Eq. 1 becomes:

$$\Delta[S]_{(r,t+\Delta t)} = D_S \cdot \Delta t \cdot \{(r + \Delta r)[S]_{(r+\Delta r,t)} - 2r[S]_{(r,t)} + (r - \Delta r)[S]_{(r-\Delta r,t)}\}/(r \cdot \Delta r^2). \quad (2)$$

To solve this equation, initial and boundary conditions must be defined. All species are assumed initially to be homogeneously distributed throughout the cell with known total concentrations of B_1, B_2, B_3, and C_0 ($[Ca^{2+}]_i$ initial). Given the equilibrium constants (K_d) for the three buffers, the initial concentrations of the species involved can be easily calculated according to the mass-action law for each individual case.

The boundary condition for the outermost shell can be obtained by considering a virtual external shell that is always in equilibrium with the outermost shell. The boundary condition at the most internal shell is obtained by setting a virtual shell at the center of the cell, always in equilibrium with the most internal shell, and by increasing the fluxes across the central sphere by a factor of 3 (Crank, 1975). The diffusion coefficient used for free calcium was $6 \cdot 10^{-6}$ cm^2/s (Hodgkin and Keynes, 1957).

Calcium buffering

The following first order kinetic scheme applies for each of the three buffer systems:

$$[C] + [B] \underset{k_-}{\overset{k_+}{\rightleftharpoons}} [C - B], \quad (3)$$

where [C] is $[Ca^{2+}]_i$, [C − B] is the concentration of Ca-bound buffer, k_+ and k_- are forward and backward binding rates, respectively. The dissociation constant (K_d) is equal to k_-/k_+.

B_1, intended to represent the natural, intrinsic buffers, is defined as a mobile, kinetically fast buffer with relatively low capacity. The characteristics of B_2 were chosen to mimic the properties of the smooth endoplasmic reticulum: immobile, slow, and with high capacity (Rasgado-Flores and Blaustein, 1987).

The effect of buffering on the concentration of the different species is given by differential equations derived from scheme 3 for each case. Then, the difference equations for any buffer system take the form:

$$\Delta[C]^B_{(t+\Delta t)} = \{k_- \cdot [C - B]_{(t)} - k_+ \cdot [C]_{(t)} \cdot [B]_{(t)}\} \cdot \Delta t \quad (4)$$

$$\Delta[B]^B_{(t+\Delta t)} = \Delta[C]^B_{(t+\Delta t)} \quad (5)$$

$$\Delta[C - B]^B_{(t+\Delta t)} = -\Delta[C]^B_{(t+\Delta t)}. \quad (6)$$

Eq. 4–6 are used independently for B_1, B_2, and B_3 (when present).

Calcium influx

The change in $[Ca^{2+}]$ due to calcium influx at the outermost shell is given by:

$$\Delta[C]^I(t) = -I_{Ca} \cdot \Delta t/(2FV) \quad (7)$$

where I_{Ca} is the transmembrane calcium current, F is Faraday's constant, and V is the volume of this compartment.

Calcium extrusion

All extrusion mechanisms (Na-dependent Ca efflux and ATP-fueled Ca pump) have been lumped as a single, voltage-independent system with Michaelian kinetics. This system is only present at the outermost shell and is described by the following difference equation:

$$\Delta[C]^P_{(t+\Delta t)} = -\{v_{max} \cdot A \cdot \Delta t \cdot [C]_{(t)}\}/\{V \cdot ([C]_{(t)} + K_m)\}, \quad (8)$$

where v_{max} is the maximal velocity of transport (in moles per surface and time units), A is the area of the cell, V is the volume of the outermost shell, and K_m is the half-maximal activating concentration.

Leakage

Because the pumping system operates constantly, a steady leakage of calcium into the outermost shell is needed to maintain a fixed $[Ca^{2+}]_i$ at rest. The amount of calcium leakage is given by:

$$\Delta[C]^L = (v_{max} \cdot A \cdot \Delta t \cdot [C]_0/\{V \cdot ([C]_0 + K_m)\}. \quad (9)$$

Integration

The concentration of the different species at each shell is given by the following equations:

$$[B_1]_{(r,t+\Delta t)} = [B_1]_{(r,t)} + \Delta[B_1]^B_{(r,t+\Delta t)} + \Delta[B_1]^D_{(r,t+\Delta t)} \quad (10)$$

$$[C - B_1]_{(r,t+\Delta t)} = [C - B_1]_{(r,t)} + \Delta[C - B_1]^B_{(r,t+\Delta t)} + \Delta[C - B_1]^D_{(r,t+\Delta t)} \quad (11)$$

$$[B_2]_{(r,t+\Delta t)} = [B_2]_{(r,t)} + \Delta[B_2]^B_{(r,t+\Delta t)} \quad (12)$$

$$[C - B_2]_{(r,t+\Delta t)} = [C - B_2]_{(r,t)} + \Delta[C - B_2]^B_{(r,t+\Delta t)} \quad (13)$$

$$[B_3]_{(r,t+\Delta t)} = [B_3]_{(r,t)} + \Delta[B_3]^B_{(r,t+\Delta t)} + \Delta[B_3]^D_{(r,t+\Delta t)} \quad (14)$$

$$[C - B_3]_{(r,t+\Delta t)} = [C - B_3]_{(r,t)} + \Delta[C - B_3]^B_{(r,t+\Delta t)} + \Delta[C - B_3]^D_{(r,t+\Delta t)} \quad (15)$$

$$[C]_{(r,t+\Delta t)} = [C]_{(r,t)} + \Delta[C]^{B1}_{(r,t+\Delta t)} + \Delta[C]^{B2}_{(r,t+\Delta t)} + \Delta[C]^{B3}_{(r,t+\Delta t)} + \Delta[C]^D_{(r,t+\Delta t)} + \Delta[C]^I_{(t+\Delta t)} + \Delta[C]^P_{(t+\Delta t)} + \Delta[C]^L. \quad (16)$$

The last three terms in eq. 16 take values different from 0 only at the outermost shell. Terms with superscript D come from Eq. 2, with superscript B from Eqs. 5 or 6, with superscripts B_1, B_2, and B_3 from the application of Eq. 4 to each buffer system, and those with superscripts I, P, and L come from Eqs. 7, 8, and 9, respectively. Unless otherwise indicated, all parameters took the values listed in Table 1. It is assumed that bound and unbound buffers have the same diffusion coefficient.

Both simulations and data analysis were conducted on a workstation (Sun Microsystems Inc., Mountain View, CA) with programs written in C language.

RESULTS

Spatiotemporal distribution of $[Ca^{2+}]_i$

Fig. 3 *B* illustrates the theoretical Ca^{2+} transients obtained at 0.25, 5, 10, and 20 μm underneath the membrane of a 20-μm-radius model cell. The characteristics of Ca^{2+} buffering and transport were similar to those that mimicked the Ca^{2+} transients monitored with confo-

cal microscopy, of a bullfrog sympathetic ganglion neuron under voltage-clamp conditions (Hernández-Cruz et al., 1989*a* and *b*). As in those experiments, a standard 100-ms-duration pulse was used. All the parameters are listed in Table 1. In the model, $[Ca^{2+}]_i$ dynamics show two different phases. During the first phase lasting ~1 s, strong spatial gradients are present throughout the cell. The time course of this fast redistribution of Ca^{2+} is dominated by diffusional processes. During the second phase, $[Ca^{2+}]_i$ has equilibrated across the cell, and the subsequent time course of decay depends on slow buffering and extrusion.

The shape of the calcium transients at different positions in the cell is strongly dependent on several variables whose influence is studied below.

Pulse duration

In general, neurons are capable of generating sustained firing, producing relatively large calcium loads. The influence of pulse duration on Ca transients at different locations in the cell is shown in Fig. 1, where pulses 10, 50, and 200 ms in duration are compared (see also 100-ms pulse in Fig. 3 *B*). As expected, the longer the pulses, the larger and faster the calcium signals. The redistribution rate of Ca^{2+} occurring during the first phase is not much affected by the pulse duration. However the time course of this first phase can be substantially altered if the Ca^{2+} entry during the pulse is large enough to saturate the buffers, allowing free calcium to diffuse and equilibrate faster (not shown).

TABLE 1 Parameters used in simulations

Cell radius	20 μm
Ca^{2+}	
$[C]_0$	0.05 μM
D_{Ca}	$6 \cdot 10^{-6}$ cm^2/s
Fast buffer (B_1)	
$[B_1]_{total}$	100 μM
k_+	10^8 M$^{-1} \cdot$ s^{-1}
K_d	1 μM
D_{B1}	$0.5 \cdot 10^{-6}$ cm^2/s
Slow buffer (B_2)	
$[B_2]_{total}$	600 μM
k_+	$5 \cdot 10^5$ M$^{-1} \cdot$ s^{-1}
K_d	0.4 μM
D_{B2}	0
Membrane extrusion	
v_{max}	2 pmol/cm$^2 \cdot$ s
K_m	0.83 μM
Stimulus	
I_{Ca}	5 nA
Duration	100 ms
Calculation steps	
Δx	0.5 μm
Δt	0.1 ms
	0.005 ms*

*Only used for Eq. 4.

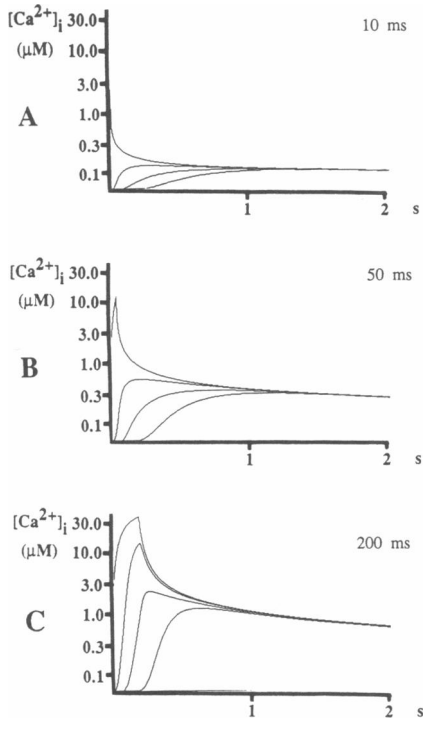

FIGURE 1 Effect of pulse duration. Simulations of Ca^{2+} transients after 10 (*A*), 50 (*B*), and 200 ms (*C*) calcium entry pulses. Other parameters are as in Table 1. Different profiles in each panel correspond (from the earliest to the latest) to Ca^{2+} transients at shells positioned 0.25 (outermost), 5, 10, and 20 μm underneath the membrane.

Fig. 2 shows the relationship between pulse duration and peak $[Ca^{2+}]_i$ reached at different depths. The size of the transients depends on the calcium load, but the relationship is not linear. For instance, peak $[Ca^{2+}]_i$ at the outermost shells, which is always higher than anywhere else, increases gradually with pulse durations up to ~10 ms. Then the slope becomes steeper up to ~100 ms, where it seems to flatten again. This can be explained as follows: When the fast buffer (B_1) begins to saturate (i.e., pulse durations of ~10 ms) a greater proportion of calcium is free, explaining the steeper slope. But when the calcium load is large enough (i.e., pulse durations of ~100 ms), $[Ca^{2+}]$ reaches values so high that the effect of slow buffers (B_2) becomes of consequence. As free B_1 gets depleted in the outer shells, Ca^{2+} diffuses much faster toward the center. Thus, the relationship between pulse duration and peak $[Ca^{2+}]_i$ appears to be steeper at deeper locations into the cell.

Fast buffering

Although the existence of endogenous fast buffering of Ca^{2+} in the cytosol has not been directly demonstrated,

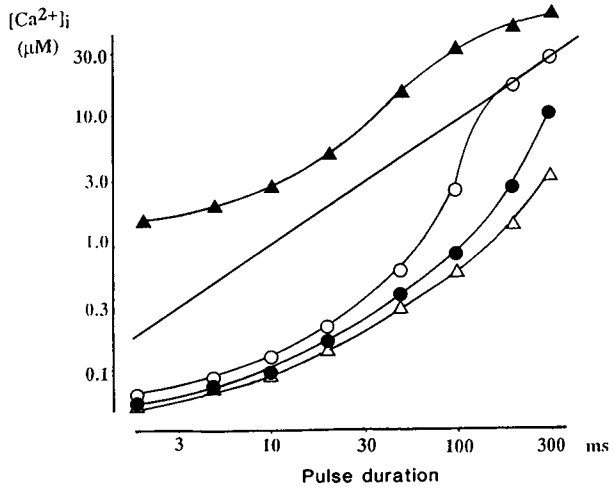

FIGURE 2 Relationship between peak $[Ca^{2+}]_i$ and pulse duration at different shells. Closed triangles correspond to the outermost shell (0.25 μm from the membrane). Open circles, closed circles, and open triangles correspond to shells positioned at 5, 10, and 20 μm underneath the membrane, respectively. Straight line represents the relation expected in the absence of buffering, extrusion, and diffusion.

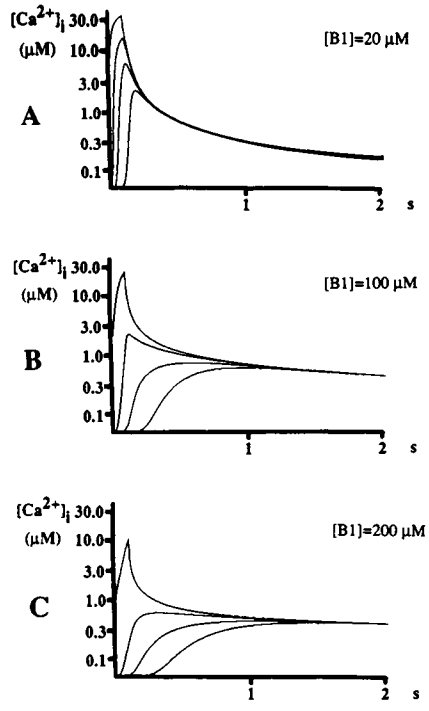

FIGURE 3 Effect of fast buffer concentration. Simulations of Ca^{2+} transients in the presence of 20 (*A*), 100 (*B*), and 200 μM (*C*) of kinetically fast buffer. Other parameters are as in Table 1. Different profiles in each panel correspond (from the earliest to the latest) to Ca^{2+} transients at shells positioned 0.25 (outermost), 5, 10, and 20 μm underneath the membrane.

strong suggestions in favor of this possibility exist (Ahmed and Connor, 1988). Ca^{2+} transients measured with confocal microscopy and fluorescent Ca indicators are often much smaller than predicted if the dye is the only fast calcium buffer (Hernández-Cruz et al., 1989*a* and *b*; Hernández-Cruz, A., and F. Sala, unpublished results). In addition, the existence of high concentrations of calmodulin and calcineurin has been demonstrated in nervous tissue (Wood et al., 1980), and the kinetics of these calcium-binding proteins has been found to be quite fast (Robertson et al., 1980). The buffering role of such calcium-binding proteins might be of minor importance compared with their function in the processing of Ca-triggered signals (Carafoli, 1987), but it is clear that at the concentrations reported (Watterson et al., 1980) they may buffer calcium because of their high affinity and fast kinetics.

Capacity

First, we considered the effect of varying the amount of kinetically fast Ca-buffering system (B_1) with all other parameters listed in Table 1 unchanged. Increasing $[B_1]$ has the expected effect of reducing peak $[Ca^{2+}]_i$ after pulses of any duration and at every location. Also, the time course of the Ca^{2+} signal changes depending on $[B_1]$. Fig 3 shows $[Ca^{2+}]$ temporal profiles at the same locations as in Fig. 1 but with either 20, 100, or 200 μM of B_1. With 20 μM of buffer, $[Ca^{2+}]$ peaks quickly at all locations and then decays rapidly. In contrast, 200 μM of buffer prolongs the redistribution phase from ~200 ms to >1 s, and the subsequent decay is slowed. Therefore, the presence of buffer not only considerably delays the arrival of raised $[Ca^{2+}]_i$ to the cell interior, but also prolongs the time to which the calcium level remains increased. This can be explained if Ca^{2+} buffered by the fast systems remains, to a degree, inaccessible to uptake by the slow, high-capacity buffer B_2 which represents intracellular storage pools in the model. The effects of increasing buffer capacity were exaggerated when mobility was simultaneously reduced (see below).

Mobility

Most calcium diffusion models assume that the buffer is unsaturable, infinitely fast, and immobile (Zucker and Stockbridge, 1983; Stockbridge and Moore, 1984; Fogelson and Zucker, 1985; but see also Connor and Nikolakopoulou, 1982; and Simon and Llinás, 1985). Some of these models were designed to simulate transmitter release kinetics where the influence of buffer mobility is expected to be small in the ranges of space and time required for evoked transmitter release (Simon and Llinás, 1985). Nevertheless, the putative buffers are soluble with a relatively low molecular weight (Carafoli, 1987),

and therefore they may diffuse. It seems then reasonable to explore the influence of their mobility on the time course of Ca^{2+} signals after relatively long stimuli and/or on a broader spatial scale.

Fig. 4 shows the Ca^{2+} transients obtained in simulations where the mobility of B_1 has been varied. It can be seen that by increasing the mobility of B_1 (Fig. 4 *C*) the first phase becomes slightly shortened. More striking effects are seen when the buffer is made immobile (Fig. 4 *A*). When Fig. 4, *A* and *B*, are compared, it can be seen that Ca^{2+} transients at 0.25 and 5 μm underneath the membrane are not too dissimilar, but those at deeper shells are markedly different: the redistribution phase in Fig. 4 *A* takes >2 s to complete, and the final Ca^{2+} levels reached are smaller. It is clear from these simulations that calcium not only diffuses by itself, but also bound to the mobile buffer molecules. Thus, the mobility of the buffer determines to great extent the time course of the redistribution phase. When Ca^{2+} binds to the buffer in the outer shells, two spatial gradients are formed: an inward gradient of Ca-buffer complex, and an outward gradient of free buffer. As the Ca-buffer complex moves inward, it releases calcium because the equilibrium between the bound and unbound forms has changed. Thus if the backward binding rate (k_-) of B_1 is made smaller, then $[Ca^{2+}]$ rises much more slowly at deeper shells (not shown).

Kinetics

In principle, cells could have different types of fast Ca-binding molecules with different capacity and kinetics. Their average behavior could be approached by considering a single buffer system, and the relative proportion of each type could be simulated by changing the kinetic properties of the whole system. Fig. 5 shows the effect of setting the dissociation constant of B_1 either at 0.25 μM (*A*), at 1 μM (*B*), or at 5 μM (*C*). Increasing the K_d of B_1 has several effects: (*a*) The rise in $[Ca^{2+}]_i$ in the cell interior after Ca entry is speeded up. (*b*) There is also an increase in the peak $[Ca^{2+}]_i$ reached in deeper shells. (*c*) The redistribution phase is shortened. (*d*) $[Ca^{2+}]_i$ decays much faster during the second phase. When buffers have low affinity, a larger proportion of calcium remains free, explaining effects *a* and *b*. Because Ca^{2+} can diffuse faster, the spatial gradients dissipate at earlier times. This explains effect *c* and also why effects *a* and *b* are more noticeable in the cell interior. Effect *d* could be

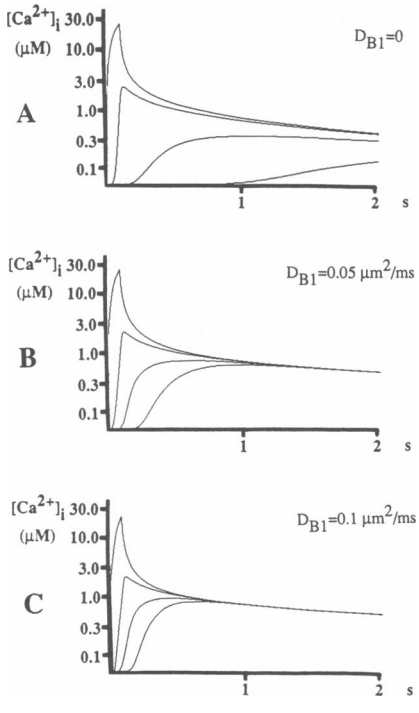

FIGURE 4 Effect of buffer mobility. Simulations of Ca^{2+} transients in the presence of kinetically fast buffers with different mobility. Diffusion coefficients are 0 (*A*), 0.5 (*B*), and 1 $\cdot 10^{-6}$ cm^2/s (*C*). Other parameters are as in Table 1. Different profiles in each panel correspond (from the earliest to the latest) to Ca^{2+} transients at shells positioned 0.25 (outermost), 5, 10, and 20 μm underneath the membrane.

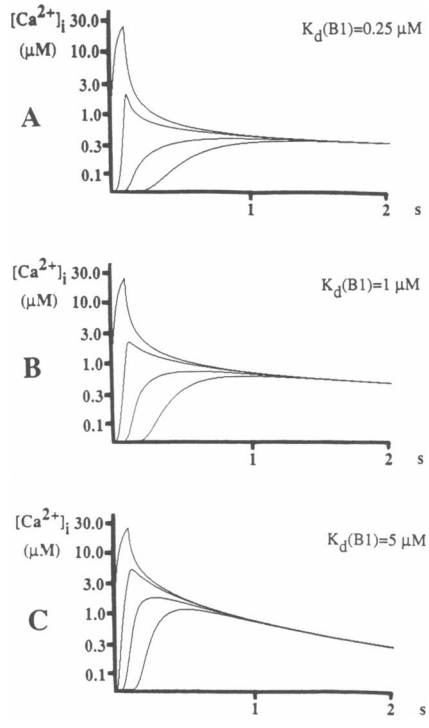

FIGURE 5 Effect of buffer affinity. Simulations of Ca^{2+} transients in the presence of kinetically fast buffers with different affinity. Dissociation constants are 0.25 (*A*), 1 (*B*), and 5 μM (*C*). Other parameters are as in Table 1. Different profiles in each panel correspond (from the earliest to the latest) to Ca^{2+} transients at shells positioned 0.25 (outermost), 5, 10, and 20 μm underneath the membrane.

interpreted in terms of a competition between two buffer systems, B_1 and B_2, the latter with higher affinity and capacity but with much lower forward binding rate. In the simulations shown, K_d was increased by means of increasing the backward binding rate. However, exactly the same effect is observed if K_d is changed by decreasing the forward binding rate.

Slow buffering

Calcium flux measurements in synaptosomes indicate the existence of a high capacity, slow uptake mechanism in cytoplasm (Rasgado-Flores and Blaustein, 1987). Such a mechanism is likely to correspond to the smooth endoplasmic reticulum or calciosomes (Volpe et al., 1988). The presence of a buffering system with slow kinetics is necessary to explain the decay phase of $[Ca^{2+}]_i$ seen in Ca^{2+} imaging experiments (Thayer et al., 1988; Lipscombe et al., 1988*b*; Hernández-Cruz et al., 1989*a* and *b*). We modeled this sequestration process (B_2) based on data reported by Rasgado-Flores and Blaustein (1987). Fig. 6 shows the effect of either removing or doubling the capacity of B_2 in all shells. Two main effects are visible when B_2 is present: (*a*) A reduction in peak $[Ca^{2+}]_i$; and (*b*) an acceleration in the time course of decay during the second phase (in fact the decay is practically absent when B_2 is removed). The first effect (i.e., reduction of peak $[Ca^{2+}]_i$ from 6.75 to 1.97 μM at 5 μm from the membrane in the presence of 600 μM of B_2) is apparent only when the calcium influx is large enough. For instance, there is no effect if the pulse lasts 20 ms or less. However the speeding of the decay phase is independent of the size of the Ca^{2+} load. The effect on the late phase is more visible if the concentration of intrinsic fast buffer is lowered (not shown).

Calcium extrusion

Fig. 7 shows Ca^{2+} transients when the extrusion mechanism at the membrane adopts several rates. The presence of a pump with a maximal rate of 2 pmol/cm^2·s as reported by Blaustein (1977) and with a K_m as low as 0.83 μM has little or no effect on the shape of the transients (Fig. 7 *B*). It is only when the rate is increased 10 times (Fig. 7 *C*), that the effect of pumping becomes apparent,

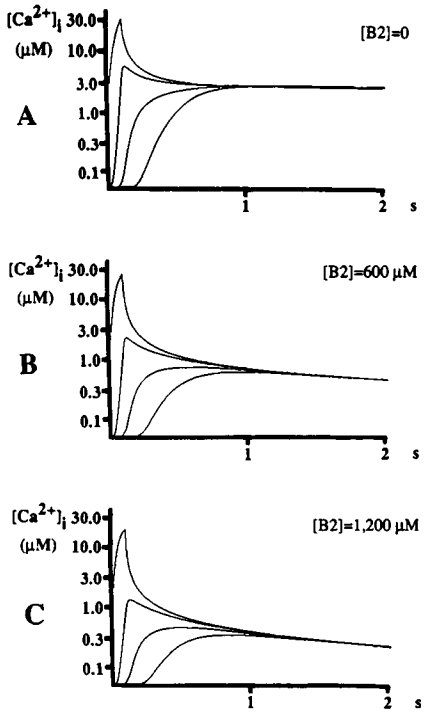

FIGURE 6 Effect of slow buffer capacity. Simulations of Ca^{2+} transients in the presence of different amounts of kinetically slow and immobile buffer (B_2). [B_2] are 0 (*A*), 600 (*B*), and 1,200 μM (*C*). Other parameters are as in Table 1. Different profiles in each panel correspond (from the earliest to the latest) to Ca^{2+} transients at shells positioned 0.25 (outermost), 5, 10, and 20 μm underneath the membrane.

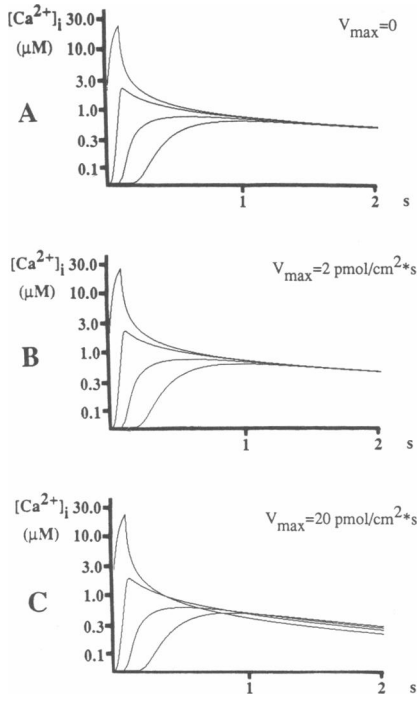

FIGURE 7 Effect of maximal extrusion rate. Simulations of Ca^{2+} transients in the presence of a membrane Ca^{2+} extrusion mechanism with different maximal rates: 0 (*A*), 2 (*B*), and 100 pmol/cm^2 · s (*C*). Other parameters are as in Table 1. Different profiles in each panel correspond (from the earliest to the latest) to Ca^{2+} transients at shells positioned 0.25 (outermost), 5, 10, and 20 μm underneath the membrane.

and it is even more evident after a 50-fold increase (not shown). The global effect consists in decreasing the peak $[Ca^{2+}]_i$ and accelerating the rate of decay at all locations in the cell, thereby creating a spatial gradient toward the periphery, as can be seen at later times in Fig. 7 *C*.

The model results that the contribution of the pump is small suggests that measured maximum effluxes are underestimated (see Discussion; see also Stockbridge and Moore [1984]).

Presence of dyes

The introduction of Ca^{2+} imaging has provided a useful tool in the study of intracellular calcium dynamics (Tsien, 1988). Because Ca^{2+} indicators are needed in these studies, and they behave as Ca buffers themselves, we examined the influence that these indicators could have on the Ca^{2+} signals. Fortunately we know (or can closely approximate) the main parameters (capacity, mobility, and kinetics) of these exogenous buffers. We simulated the presence of either 20 or 100 μM of fura-2 (Grynkiewicz et al., 1985) by adding an additional buffer system (B_3) to the parameters listed in Table 1. We assumed a forward binding rate of 10^8 $M^{-1} \cdot s^{-1}$ and a dissociation constant of 0.2 μM (Jackson et al., 1987; Klein et al., 1988; Kao and Tsien, 1988). A diffusion coefficient (D_{B3}) of $5 \cdot 10^{-6}$ cm^2/s was found for fura-2 in aqueous solution (Timmermann and Ashley, 1986), whereas a value 10 times smaller has been reported in skeletal muscle fibers (Timmermann and Ashley, 1986; Konishi et al., 1988). Such a decrease has been attributed to a higher viscosity (Timmermann and Ashley, 1986) and/or to intracellular binding (Konishi et al., 1988). In contrast, there seems to be no significant binding of fura-2 in cytoplasm of smooth muscle cells (Williams et al., 1985). We have assumed a D_{B3} of $2.5 \cdot 10^{-6}$ cm^2/s, a larger value than reported for skeletal muscle, because it better fitted experimental data (Hernández-Cruz et al., 1989*a* and *b*) obtained with fluo-3 and rhod-2 which are Ca indicators of similar molecular weight, and because the viscosity and binding to intracellular proteins in bullfrog neurons are likely to be lower than in skeletal muscle cells.

The addition of fura-2 to the model changes the transients to a different extent depending on dye concentration (see Fig. 8). If total fura-2 concentration is 20 μM, Ca^{2+} signals are only slightly smaller and the duration of the redistribution phase is somewhat shorter. Nonetheless, more obvious effects are found in the presence of 100 μM of fura-2. In addition, the second phase of $[Ca^{2+}]_i$ decay is slowed because of binding to dye.

The fact that in the presence of dye the redistribution of calcium is shortened can be easily explained because fura-2 is a relatively fast diffusible molecule and therefore carries Ca toward the center. According to this explanation, the dye would tend to mask the calcium carrying ability of the mobile and kinetically fast intrinsic buffers. Can any conclusion about the mobility of intrinsic buffers be drawn from experiments conducted in the presence of mobile dyes? Fig. 9 demonstrates that this depends on the dye concentration. Two different situations have been simulated differing only in the mobility of the intrinsic buffer B_1 ($D_{B1} = 10^{-6} cm^2/s$ or $D_{B1} = 0$), and the temporal profiles are found to be easily distinguishable (Fig. 9 *A*). When 20 μM of fura-2 is added, the profiles change but they still could be distinguished (Fig. 9 *B*). That is no longer true in the presence of 100 μM (a concentration typically used in Ca measurement experiments) where the dye mobility completely masks the otherwise slow Ca^{2+} diffusion due to the existence of stationary buffer and the profiles are similar regardless of the intrinsic buffer mobility (Fig. 9 *C*). It should be pointed out that these masking effects of the dye do not depend on the absolute amount of dye but only on its proportion relative to the intrinsic buffers. The bigger the ratio, the larger the distorting effects become.

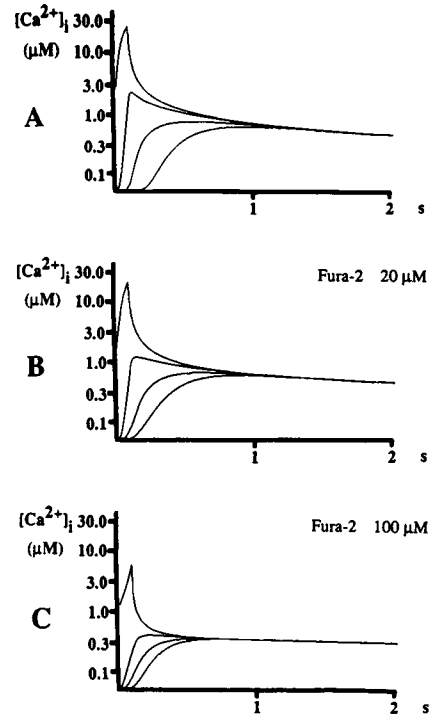

FIGURE 8 Effect of addition of the Ca^{2+} indicator fura-2. Simulations of Ca^{2+} transients in the presence of 20 (*B*) and 100 μM (*C*) of fura-2. (*A*) Control simulation with all the parameters as listed in Table 1. Parameters of fura-2 (B_3) are: $k_+ = 10^8$ $M^{-1} \cdot s^{-1}$, $K_d = 0.2$ μM, and $D_{B3} = 2.5 \cdot 10^{-6}$ cm^2/s. Different profiles in each panel correspond (from the earliest to the latest) to Ca^{2+} transients at shells positioned 0.25 (outermost), 5, 10, and 20 μm underneath the membrane.

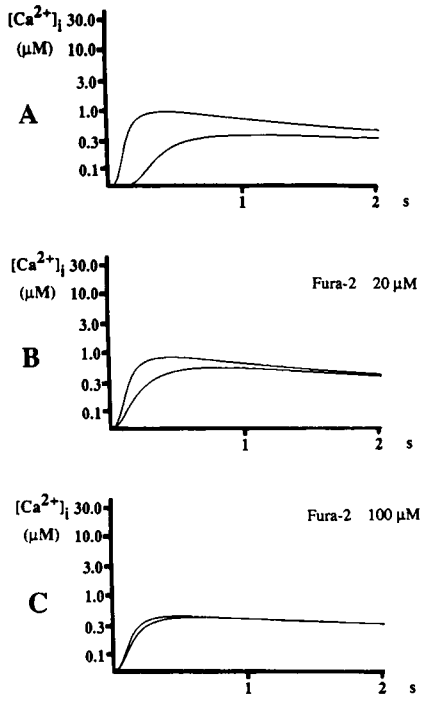

FIGURE 9 Masking effects of exogenous buffer addition. Simulations of Ca^{2+} transients at the shell positioned 10 μm underneath the membrane in the absence (*A*) or in the presence of 20 (*B*) and 100 μM (*C*) of fura-2. Fura-2 characteristics are as in Fig. 8. All parameters except buffer mobility (D_{B1}) are as listed in Table 1. For all panels the top trace correspond to a buffer diffusion coefficient of $1 \cdot 10^{-6}$ cm^2/s. The bottom trace simulation is when B_1 is immobile ($D_{B1} = 0$) for all three panels.

DISCUSSION

The present diffusion model continues the line of other intracellular calcium diffusion models previously reported for neurones, beginning with the work of Hodgkin and colleagues (Blaustein and Hodgkin, 1969; Baker et al., 1971). Most of them have focused on the study of theoretical calcium concentration near the plasma membrane after its entry through Ca channels and its relationship with either neurotransmitter release phenomena (Smith and Zucker, 1980; Zucker and Stockbridge, 1983; Stockbridge and Moore, 1984; Fogelson and Zucker, 1985; Simon and Llinás, 1985; Parnas, et. al., 1989), aequorin and arsenazo III signals (Connor and Nikolakopoulou, 1982; Tillotson and Nasi, 1988), or activation and inactivation of Ca-dependent membrane conductances (Andresen et al., 1979; Gorman and Thomas, 1980; Barish and Thompson, 1983; Yamada et al., 1989). Our model differs from others in emphasizing the importance that calcium transients may have, not only underneath the plasma membrane, but also in deeper spatial domains where calcium can activate processes of physiological relevance like intracellular calcium release (Fabiato, 1983; Lipscombe et al., 1988*b*), or gene expression (Morgan and Curran, 1988). A similar approach, but on a different spatial scale, has been used to simulate the dynamics of free calcium in dendritic spines (Gamble and Koch, 1987).

Most of the reported Ca diffusion models used a constant diffusion coefficient for calcium which has been lowered to a variable extent from its value in saline solution. This change in the apparent diffusion coefficient results from viscosity and tortuosity of the cytosolic matrix, as well as from the presence of intracellular Ca-binding buffers that slow the diffusion of ionized calcium (Connor and Nikolakopoulou, 1982). Such an approach assumes that Ca buffers are unsaturable, immobile, and much faster than any diffusion movement (Crank, 1975). Though these assumptions may be adequate for the study of Ca-dependent processes occurring near the membrane (but see Simon and Llinás, 1985), they yield results that can be equivocal when trying to simulate Ca^{2+} signals elsewhere. Therefore we have formulated a diffusion model which allows us to explore the influence of intracellular buffers in shaping intracellular Ca^{2+} signals in a spherical cell with the characteristics of a bullfrog sympathetic ganglion neuron. Formally, the model only differs in detail from that of Connor and Nikolakopoulou (1982), but ours explores in greater depth the effects of buffer mobility and kinetics on delivery of Ca^{2+} to sites deeper within the cell.

As with all models, ours is limited by unavoidable assumptions. For instance, we have not considered that calcium entry occurs at discrete points in the plasma membrane (Chad and Eckert, 1984; Simon and Llinás, 1985; Fogelson and Zucker, 1985; Zucker and Fogelson, 1986) because the large calcium gradients near the channel mouth predicted by these models could only be relevant for processes occurring in locations within the submicron spatial range and with kinetics in the submillisecond range. This reflects the fact that the mean open time of calcium channels is only ~1 ms and the large gradients produced dissipate quickly after channel closure (Simon and Llinás, 1985; Fogelson and Zucker, 1985). However, the model seems most appropriate for cells with a relatively high density of Ca channels. Our model assumes that calcium enters into the cell through uniformly distributed channels and does not take into account that calcium channels may be clustered in specialized regions of the membrane, thus creating spatial gradients that would take longer to dissipate (Thompson and Coombs, 1988; Lipscombe et al., 1988*a*). Also, for simplicity we have not incorporated other heterogeneities such as an unevenly distributed buffer (Tillotson and Gorman, 1980) or a Ca-releasing mechanism (Kuba et

al., 1983). The characterization of endogenous buffers is also incomplete. B_1 is assumed to be a single species with fast kinetics and parameters that ranged within reasonable limits. B_2 represents the slow buffering found in synaptosomes attributed to smooth endoplasmic reticulum (SER), and was incorporated under the assumption that SER also contributes to buffer Ca^{2+} in cell bodies. The values used in modeling the extrusion mechanism are also guesses (see below). In spite of all these limitations the model gives some insights in the role that buffering mechanisms could play in determining the intracellular dynamics of ionized calcium.

Calcium buffers characteristics strongly affect the size and time course of Ca^{2+} transients

The size of Ca^{2+} signals depends mostly on the calcium load and its proportion relative to the buffer capacity and its affinity. But if these two factors almost completely determine the size and duration of calcium transients in regions close to the plasma membrane, the picture is quite different for deeper regions in the cell. There, a complex interplay among capacity, mobility, and affinity of buffers decides the shape of Ca^{2+} signals.

Figs. 3–5 demonstrate how each of those parameters, independently of the others, determine when, how much, and how long free calcium remains increased at different depths. The differences are not always dramatic, but provided that they occur in the submicromolar range where many physiologically relevant processes take place, they could be important. Furthermore, differences resulting from different simulation conditions can be made larger if more than one variable of those listed in Table 1 changes at the same time. For instance, Fig. 3 *C* shows that 200 μM of B_1 with K_d = 1 μM and $D = 0.5 \cdot 10^{-6}$ cm^2/s allows $[Ca^{2+}]$ to increase up to 0.45 μM after 1 s and to remain high for several seconds 10 μm away from the membrane. In contrast, if B_1 were immobile, $[Ca^{2+}]$ would only climb to ~0.3 μM and only after several seconds (not shown). Moreover, in the case where B_1 were immobile and had a high affinity (K_d = 0.25 μM), the increase in $[Ca^{2+}]$ at 10 μm would be negligible (not shown). Thus, an adequate combination of buffer parameters may determine to what extent different regions in the cell might get exposed to perturbations in cytosolic Ca^{2+} resulting from calcium entry through the plasma membrane. This represents a potentially useful mechanism for spatial regulation of intracellular Ca signals.

Among the three parameters in the model, mobility seems to have a predominant importance because a mobile buffer can carry and release Ca^{2+} into deeper regions whereas an immobile buffer cannot do the job. However it is notable that this would be true only under certain specific circumstances. For instance, were $[B_1]$ = 20 μM or lower, or the initial $[Ca^{2+}]_i$ higher (>100 μM), or the calcium load fivefold larger, buffer mobility would not be as important. Regardless of its diffusion coefficient, the buffer would become rapidly saturated, allowing Ca^{2+} to diffuse freely into the cell (not shown). On this basis, it can be speculated that, depending on the characteristics of their Ca buffers, different types of neurons or different regions in the same neuron might shape Ca^{2+} signals in a markedly different manner. For instance a region absolutely silent to Ca entry could be produced if it were surrounded by diffusion restricted areas with high-affinity, high-capacity fast buffers which would prevent ionized calcium from moving further. If those areas existed near the plasma membrane, calcium extrusion would be also facilitated, thus making Ca^{2+} signals shorter lasting. One could speculate that such a role could be played by the subsurface cisterns of endoplasmic reticulum found in bullfrog sympathetic neurons and other neuronal types (Fujimoto et al; 1980) Another example of neuronal type-specific calcium regulation could be displayed by the calcium-binding protein parvalbumin which has been found in brain (Baron et al., 1975; Heizmann, 1980) and which seems to influence the electrical properties and enzymatic machinery which modulate excitability and activity of GABA neurons (Celio, 1986).

Slow mechanisms

In addition to the role that fast buffers play, high-affinity, high-capacity slow buffering systems are also important in terminating Ca^{2+} transients. We have not simulated the mitochondrial sequestering mechanisms which seem to possess a much lower affinity and are too slow to influence the results on the time scale relevant for these simulations. The importance of slow buffering simulated with parameters derived from data on smooth endoplasmic reticulum in synaptosomes (Rasgado-Flores and Blaustein, 1987) is demonstrated in Fig. 6, where in the absence of B_2 $[Ca^{2+}]_i$ remains above 2 μM for many seconds. In contrast with fast buffers, whose main role is to avoid large $[Ca^{2+}]$ increases after a Ca entry, slow buffers can only act in the time scale of milliseconds when the Ca^{2+} load is large enough to saturate the fast buffers. On the other hand, given their large capacity, slow buffers are mostly responsible for the termination of the Ca signal in the time scale of seconds.

It has to be pointed out that the extrusion rate of 2 $pmol/cm^2 \cdot s$ used in our simulations is probably too low. Though the parameters have been taken from squid axon data (Blaustein, 1977), the removal of an extrusion mechanism with such a rate has little effect on the calculated Ca^{2+} transients. Stockbridge and Moore

(1984) discussed the validity of the measurements of maximal rates on the basis of methodological problems. Indeed, if the time resolution is inappropriately low, the measured initial rates are diffusion limited and therefore likely to be underestimated. For instance, Pennefather and Goh (1988) reported that blockade of Na/Ca exchange by removing extracellular Na slows the decay of a voltage-independent Ca^{2+}-sensitive potassium current in bullfrog sympathetic neurons, I_{AHP}. Assuming that Na/Ca exchange contributes 60% to the maximal rate of extrusion, an efflux rate as fast as fivefold that reported by Blaustein (1977) was required to simulate in a version of our model the effect of Na removal in the kinetics of the I_{AHP} (Pennefather, P. P., F. Sala, and A. Hernández-Cruz, manuscript in preparation). However, according to the model, even with that value for the extrusion mechanism, the decay phase of $[Ca^{2+}]_i$ is mostly due to calcium buffering and not to calcium extrusion. This prediction is in agreement with experimental data from amphibian sympathetic neurons which show that caffeine-induced Ca^{2+} transients decay much more slowly in the presence of intracellular ruthenium red, an agent that presumably blocks calcium uptake, than in the absence of extracellular sodium (Marrion et al., 1989).

Distortions due to the presence of exogenous buffers

The question that always arises when using Ca indicators is to what extent the measured Ca^{2+} signals correspond to true physiological responses. That is particularly relevant for the current generation of policarboxylated dyes (fura-2, fluo-3, azo-1, indo-1, rhod-2), whose strong affinities mean that by introducing excessive amounts, it is easy to buffer cytosolic $[Ca^{2+}]_i$ significantly (Tsien, 1988). Whereas this feature might have little or no importance for some studies (i.e., assessing quantitatively $[Ca^{2+}]_i$ increases needed to trigger specific cell functions), it is crucial in the study of $[Ca^{2+}]_i$ dynamics. The combination of these dyes with higher-speed imaging has enabled the visualization of radial inward spread of Ca^{2+} in frog sympathetic ganglion neurons resulting from direct electrical stimulation (Lipscombe et al., 1988*b*). One step further was taken with the use of confocal microscopy (Fine et al., 1988), which provides better spatiotemporal resolution and allows measurement of $[Ca^{2+}]_i$ changes after shorter periods of stimulation (100 ms in Hernández-Cruz et al., 1989, *a* and *b*).

Because each of the three parameters of intrinsic buffers influence the shaping of Ca^{2+} transients, the introduction of an additional buffer which may have quite different properties could mask to a great extent the natural response of the cell. It has been shown that Ca^{2+} transients in a model cell ($[B_1] = 100\ \mu M$; $K_d = 1\ \mu M$) remain relatively unchanged in the presence of 20 μM of fura-2 ($K_d = 0.2\ \mu M$), but not when the dye concentration is 100 μM. If the intrinsic buffer were more concentrated or of higher affinity, the distortion due to the presence of dye would be smaller. These problems address the question of whether or not accurate information about the nature of intrinsic buffers may be extracted from experiments done in the presence of such Ca^{2+} indicators. One difficulty arises from the fact that if the dye is loaded from the external medium (ester form), all the intrinsic buffers remain undisturbed, but then neither the internal concentration of the dye nor the exact amount of calcium load are known. Both goals can be achieved if dyes are loaded from a patch-recording pipette in whole-cell configuration. Then the internal concentration of dye may be assumed to be the same as in the pipette, and Ca currents can be measured, but intrinsic mobile buffers may be washed out through the pipette. Nevertheless, because it is likely that diffusion coefficients of dyes are higher than those of Ca buffers, there may be a temporal window where dye is already in equilibrium and intrinsic buffers have not been significantly dialyzed. For instance, according to Pusch and Neher (1988) and assuming an access resistance of 5 MΩ, and molecular weights of 500 and 25,000 for dye and intrinsic buffer, respectively, the time constants for exchange between pipette and cytoplasm would be 6.8 and 25.3 min for dye and buffer, respectively, for a spherical neuron of 20 μM in radius.

It is not easy to determine the capacity and affinity of intrinsic fast buffers by analyzing and fitting experimental Ca^{2+} transients to the model. Even when other mechanisms could be eliminated under certain experimental conditions (poisoning SER and ATP-dependent uptaking processes, and removing sodium from the external medium), there exist several capacity/affinity pairs that could account for most of the experimental results. In the presence of a considerable amount of high-affinity dye, Ca^{2+} signals would be similar regardless of the existence of either high-affinity, low-capacity buffer or low-affinity, high-capacity buffer. However these two extreme situations may be distinguished if the amount of dye is relatively small. In this case high-affinity, low-capacity buffer might become nearly saturated close to the membrane and Ca^{2+} signals in these spatial domains would be larger during the redistribution phase. If the dye has the appropriate dissociation constant the difference should be detected. In addition, the model predicts that in the presence of SER and/or extrusion mechanisms, Ca^{2+} transients would be larger and decay faster at a location deeper than 10 μM if intrinsic buffer has low affinity.

The remaining property of intrinsic buffers, i.e., mobility, is harder to explore. Because dyes themselves are likely to diffuse easier than intrinsic buffers, even small amounts may become dominant in the redistribution of

Ca^{2+} during the first phase. That leads to a dilemma, because attempts to reduce this interference by means of reducing the diffusion coefficient of dyes would slow their diffusion from the pipette to the cell.

Many of these difficulties could be avoided if more efficient fluorescent Ca^{2+} indicators were available that could be used at nonperturbing concentrations. Given the extremely rapid development of the field, it is conceivable that dyes with such characteristics will be available in the foreseeable future.

We thank Dr. P. R. Adams for providing the facilities of his laboratory. Also we would like to thank Drs. P. R. Adams, J. A. Connor, and P. P. Pennefather for helpful discussion, and Mr. C. C. Choudhari for expert programming.

Dr. Sala is supported by Fundación Juan March (Spain).

Received for publication 10 May 1989 and in final form 12 October 1989.

REFERENCES

Ahmed, Z., and J. A. Connor. 1988. Calcium regulation by and buffer capacity of molluscan neurons during calcium transients. *Cell Calcium.* 9:57–69.

Andresen, M. C., A. M. Brown, and S. Yasui. 1979. The role of diffusion in the photoresponse of an extraretinal photoreceptor of *Aplysia. J. Physiol. (Lond.).* 287:283–301.

Ashcroft, F. M., and P. R. Stanfield. 1981. Calcium dependence of the inactivation of calcium currents in skeletal muscle fibers of an insect. *Science (Wash. DC).* 213:224–226.

Baker, P. F., A. L. Hodgkin, and E. B. Ridgway. 1971. Depolarization and calcium entry in squid giant axons. *J. Physiol. (Lond.).* 218:709–755.

Barish, M. E., and S. H. Thompson. 1983. Calcium buffering and slow recovery kinetics of calcium-dependent outward current in molluscan neurones. *J. Physiol. (Lond.).* 337:201–219.

Baron, G., J. Demaille, and E. Dutruge. 1975. The distribution of parvalbumins in muscle and in other tissues. *FEBS (Fed. Eur. Biochem. Soc.) Lett.* 56:156–160.

Blaustein, M. P. 1977. Effects of internal and external cations and of ATP on sodium-calcium exchange in squid axons. *Biophys. J.* 20:79–111.

Blaustein, M. P., and A. L. Hodgkin. 1969. The effect of cyanide on the efflux of calcium from squid axons. *J. Physiol. (Lond.).* 200:497–527.

Carafoli, E. 1987. Intracellular calcium homeostasis. *Annu. Rev. Biochem.* 56:395–433.

Celio, M. R. 1986. Parvalbumin in most γ-aminobutyric acid-containing neurons of the rat cerebral cortex. *Science (Wash. DC).* 231:995–997.

Chad, J. E., and R. Eckert. 1984. Calcium domains associated with individual channels can account for anomalous voltage relations of Ca-dependent responses. *Biophys. J.* 45:993–999.

Connor, J. A., and G. Nikolakopoulou. 1982. Calcium diffusion and buffering in nerve cytoplasm. *Lect. Math. Life Sci.* 15:79–101.

Crank, J. 1975. The Mathematics Of Diffusion. 2nd ed. Clarendon Press, Oxford, 414 pp.

Fabiato, A. 1983. Calcium-induced release of calcium from the cardiac sarcoplasmic reticulum. *Am. J. Physiol.* 245 (*Cell Physiol.* 14):C1–C14.

Fine, A., W. B. Amos, R. M. Durbin, and P. A. McNaughton. 1988. Confocal microscopy: applications in neurobiology. *Trends Neurosci.* 11:346–351.

Fogelson, A. L., and R. S. Zucker. 1985. Presynaptic calcium diffusion from various arrays of single channels. *Biophys. J.* 48:1003–1017.

Fujimoto, S., K. Yamamoto, K. Kuba, K. Morita, and E. Kato. 1980. Calcium localization in the sympathetic ganglion of the bullfrog and effects of caffeine. *Brain Res.* 202:21–32.

Gamble, E., and C. Koch. 1987. The dynamics of free calcium in dendritic spines in response to repetitive synaptic input. *Science (Wash. DC).* 236:1311–1315.

Gorman, A. L. F., and M. V. Thomas. 1980. Intracellular calcium accumulation during depolarization in a molluscan neurone. *J. Physiol. (Lond.).* 308:259–285.

Grynkiewicz, G., M. Poenie, and R. Y. Tsien. 1985. A new generation of Ca^{2+} indicators with greatly improved fluorescence properties. *J. Biol. Chem.* 260:3440–3450.

Heizmann, C. W. 1984. Parvalbumin, an intracellular calcium-binding protein: distribution, properties and possible roles in mammalian cells. *Experientia (Basel).* 40:910–921.

Hernández-Cruz, A., F. Sala, and P. R. Adams. 1989*a*. Subcellular dynamics of $[Ca^{2+}]_i$ monitored with laser scanned confocal microscopy in a single voltage-clamped vertebrate neuron. *Biophys. J.* 55:216a. (Abstr.)

Hernández-Cruz, A., F. Sala, and P. R. Adams. 1989*b*. Subcellular calcium transients visualized by confocal microscopy in a voltage-clamped vertebrate neuron. *Science (Wash. DC).* In press.

Hodgkin, A. L., and R. D. Keynes. 1957. Movements of labelled calcium in squid giant axons. *J. Physiol. (Lond.).* 138:253–281.

Kao, J. P. Y., and R. Y. Tsien. 1988. Ca^{2+} binding kinetics of fura-2 and azo-1 from temperature-jump relaxation measurements. *Biophys. J.* 53:635–639.

Katz, B., and R. Miledi. 1967. A study of synaptic transmission in the absence of nerve impulses. *J. Physiol. (Lond.).* 192:407–436.

Klein, M. G., B. J. Simon, G. Szucs, and M. F. Schneider. 1988. Simultaneous recording of calcium transients in skeletal muscle using high- and low-affinity calcium indicators. *Biophys. J.* 53:971–988.

Konishi, M., A. Olson, S. Hollingworth, and S. M. Baylor. 1988. Myoplasmic binding of fura-2 investigated by steady-state fluorescence and absorbance measurements. *Biophys. J.* 54:1089–1104.

Kuba, K., K. Morita, and M. Nohmi. 1983. Origin of calcium ions involved in the generation of a slow afterhyperpolarization in bullfrog sympathetic neurones. *Pfluegers Arch. Eur. J. Physiol.* 399:194–202.

Jackson, A. P., M. P. Timmerman, C. R. Bagshaw, and C. C. Ashley. 1987. The kinetics of calcium binding to fura-2 and indo-1. *FEBS (Fed. Eur. Biochem. Soc.) Lett.* 216:35–39.

Lipscombe, D., D. V. Madison, M. Poenie, H. Reuter, R. Y. Tsien, and R. W. Tsien. 1988*a*. Spatial distribution of calcium channels and cytosolic calcium transients in growth cones and cell bodies of sympathetic neurons. *Proc. Natl. Acad. Sci. USA.* 85:2398–2402.

Lipscombe, D., D. V. Madison, M. Poenie, H. Reuter, R. W. Tsien, and R. Y. Tsien. 1988*b*. Imaging of cytosolic Ca^{2+} transients arising from Ca^{2+} stores and Ca^{2+} channels in sympathetic neurons. *Neuron.* 1:355–365.

Llinás, R., I. Z. Steinberg, and K. Walton. 1981. Relationship between

presynaptic calcium current and postsynaptic potential in squid giant synapse. *Biophys. J.* 33:323–351.

Marrion, N. V., S. J. Marsh, B. J. Burbach, D. A. Brown, and P. R. Adams. 1989. Effect of ruthenium red and ryanodine on the caffeine-induced rise of intracellular calcium in vertebrate sympathetic neurons. *Soc. Neurosci. Abstr.* 15 (part I). 16 pp.

Meech, R. W. 1978. Calcium-dependent potassium activation in nervous tissues. *Annu. Rev. Biophys. Bioeng.* 7:1–18.

Morgan, J. I., and T. Curran. 1988. Calcium as a modulator of the intermediate-early gene cascade in neurons. *Cell Calcium.* 9:303–311.

Parnas, H., G. Hovav, and I. Parnas 1989. Effect of Ca^{2+} diffusion on the time course of neurotransmitter release. *Biophys. J.* 55:859–874.

Pennefather, P. P., and J. W. Goh. 1988. Relationship between calcium load and the decay rate of I_{AHP} in bullfrog ganglion neurons. *Soc. Neurosci. Abstr.* 14:1089.

Pusch, M., and E. Neher. 1988. Rates of diffusional exchange between small cells and a measuring patch pipette. *Pfluegers Arch. Eur. J. Physiol.* 411:204–211.

Rasgado-Flores, H., and M. P. Blaustein. 1987. ATP-dependent regulation of cytoplasmic free calcium in nerve terminals. *Am. J. Physiol. (Cell physiol.* 21): C588–C594.

Rasmussen, H., and P. Q. Barrett. 1984. Calcium messenger system: an integrated view. *Physiol Rev.* 64:939–984.

Robertson, S. P., J. D. Johnson, and J. D. Potter. 1980. The time-course of Ca^{2+} exchange with calmodulin, troponin, parvalbumin, and myosin in response to transient increases in Ca^{2+}. *Biophys. J.* 34:559–569.

Simon, S. M., and R. R. Llinás. 1985. Compartmentalization of the submembrane calcium activity during calcium influx and its significance in transmitter release. *Biophys. J.* 48:485–498.

Smith, G. D. 1985. Numerical solution of partial differential equations. Finite difference methods. 3rd ed. Clarendon Press, Oxford. 337 pp.

Smith, S. J., and R. S. Zucker. 1980. Aequorin response facilitation and intracellular calcium accumulation in molluscan neurones. *J. Physiol. (Lond.).* 300:167–196.

Stockbridge, N., and J. W. Moore, 1984. Dynamics of intracellular calcium and its possible relationship to phasic transmitter release and facilitation at the frog neuromuscular junction. *J. Neurosci.* 4:803–811.

Thayer, S. A., L. D. Hirning, and R. J. Miller. 1988. The role of caffeine-sensitive calcium stores in the regulation of the intracellular free calcium concentration in rat sympathetic neurons in vitro. *Mol. Pharmacol.* 34:664–673.

Thompson, S., and J. Coombs. 1988. Spatial distribution of Ca currents in molluscan neuron cell bodies and regional differences in the strength of inactivation. *J. Neurosci.* 8:1929–1939.

Tillotson, D., and A. L. F. Gorman. 1980. Non-uniform Ca^{2+} buffer distribution in a nerve cell body. *Nature (Lond.).* 286:816–817.

Tillotson, D., and E. Nasi. 1988. Ca^{2+} diffusion in the cytoplasm of *Aplysia* neurons: its relationship to local concentration changes. *In* Calcium channels and ion modulation. Plenum Publishing Corp., New York. 133–146.

Timmerman, M. P., and C. C. Ashley. 1986. Fura-2 diffusion and its use as an indicator of free calcium changes in single striated muscle cells. *FEBS (Fed. Eur. Biochem. Soc.) Lett.* 209:1–8.

Tsien, R. Y. 1988. Fluorescence measurement and photochemical manipulation of cytosolic free calcium. *Trends Neurosci.* 11:419–424.

Volpe, P., K.-H. Krause, S. Hashimoto, F. Zorzato, T. Pozzan, J. Meldolesi, and D. P. Lew. 1988. "Calciosome," a cytoplasmic organelle: the inositol 1,4,5-triphosphate-sensitive Ca^{2+} store of non-muscle cells? *Proc. Natl. Acad. Sci. USA.* 85:1091–1095.

Watterson, D. M., P. A. Mendel, and T. C. Vanaman. 1980. Comparison of calcium-modulated proteins from vertebrate brains. *Biochemistry.* 19:2672–2676.

Williams, D. A., K. E. Fogarty, R. Y. Tsien, and F. S. Fay. 1985. Calcium gradients in single smooth muscle cells revealed by the digital imaging microscope using Fura-2. *Nature (Lond.).* 318:558–561.

Wood, J. G., R. W. Wallace, J. N. Whitaker, and W. Y. Cheung. 1980. Immunocytochemical localization of calmodulin and a heat-labile calmodulin-binding protein (CaM-BP80) in basal ganglia of mouse brain. *J. Cell Biol.* 84:66–76.

Yamada, W. M., C. Koch, and P. R. Adams. 1989. Multiple channels and calcium dynamics. *In* Methods in Neuronal Modeling: From Synapses to Networks. C. Koch and I. Segev, editors. MIT Press, Cambridge, MA. 97–133.

Zucker, R. S., and A. L. Fogelson. 1986. Relationship between transmitter release and presynaptic calcium influx when calcium enters through discrete channels. *Proc. Natl. Acad. Sci. USA.* 83:3032–3036.

Zucker, R. S., and N. Stockbridge. 1983. Presynaptic calcium diffusion and the time courses of transmitter release and synaptic facilitation at the squid giant synapse. *J. Neurosci.* 3:1263–1269.